JACS
JOURNAL OF THE AMERICAN CHEMICAL SOCIETY
Article
pubs.acs.org/JACS

Reaction Parameters Influencing Cobalt Hydride Formation Kinetics: Implications for Benchmarking H_2-Evolution Catalysts

Noémie Elgrishi, Daniel A. Kurtz, and Jillian L. Dempsey*

Department of Chemistry, University of North Carolina, Chapel Hill, North Carolina 27599-3290, United States

Supporting Information

ABSTRACT: The need for benchmarking hydrogen evolution catalysts has increasingly been recognized. The influence of acid choice on activity is often reduced to the overpotential for catalysis. Through the study of a stable cobalt hydride complex, we demonstrate the influence of acid choice, beyond pK_a, on the kinetics of hydride formation. A linear free energy relationship between acid pK_a and second-order rate constants is observed for weaker acids. For stronger acids, however, further increases in pK_a do not correlate to increases in rate constants. Further, steric bulk around the acidic proton is shown to influence rate constants dramatically. Together, these observations reveal the complex factors dictating catalyst performance.

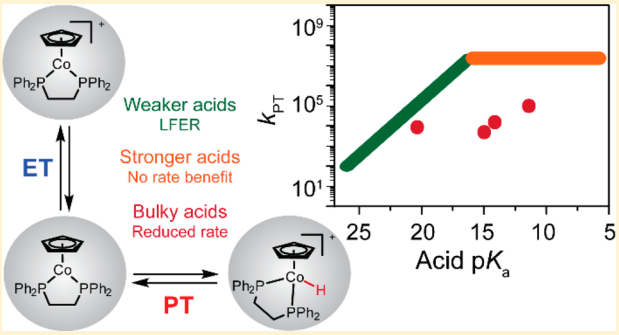

INTRODUCTION

Recent advances in the field of solar energy storage have spurred renewed interest in the elementary chemical steps involving the movements of protons and electrons in fuel-forming reactions. The underlying proton-coupled electron transfer (PCET) processes rely on transition metal catalysts to orchestrate the transformations necessary to convert small molecules to energy dense fuels.[1−4] The first and common PCET reaction pertaining to various domains of catalysis is the formation of a metal hydride, while the subsequent chemical steps differ depending on the product formed.

The formation of metal hydrides can proceed through several PCET pathways described in Scheme 1A. The electron transfer

Scheme 1

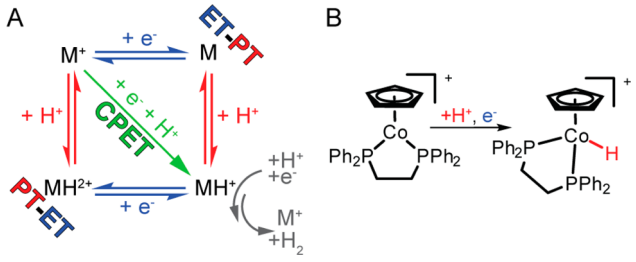

(ET) and proton transfer (PT) steps can occur sequentially, in either PT-ET or ET-PT pathways following the edges of the square scheme. Another possibility is the synchronous movement of an electron and a proton following a concerted proton−electron transfer (CPET) process. The elusive CPET pathway involving a metal hydride complex was recently identified by Hammarström with a tungsten hydride complex.[5] As hydride formation has been invoked as the rate-limiting step for a number of hydrogen evolution catalysts of first-row transition metals,[6−12] understanding the PCET reaction mechanisms associated with this, as well as other, elementary reaction steps is critical.[10,11,13,14] However, in the search for efficient catalysts, product evolution and turnover frequencies take the spotlight. As a result, elementary reaction steps remain underexplored and little is known about the parameters influencing the formation of transition metal hydrides in molecular catalysts.

Recent reports have used electrochemical techniques combined with modeling and density functional theory to probe the presence of cobalt and nickel hydride intermediates in catalytic cycles.[10,11,15−17] However, the high reactivity of metal hydride intermediates in catalytic cycles, apparent by the dearth of reports of isolated first-row transition metal hydrides,[18,19] has precluded a systematic experimental study of hydride formation reactions. In response, we set out to investigate the parameters influencing the hydride formation step, focusing on the proton source and its effect on reactivity. Understanding the parameters governing such transformations will open new avenues of research, allowing underperforming H_2-evolving catalysts to be revisited and broadening the narrow pool of high-performing hydrogen evolution reaction (HER) catalysts.

In this paper we describe the reactivity of a first-row transition metal complex to form a stable metal hydride when reduced in the presence of a proton source. Our model system, $[Co(Cp)(dppe)]^{2+}$ is based on a cobalt cyclopentadienyl (Cp) 1,2-bis(diphenylphosphino)ethane (dppe) complex which can react to form one of the very few stable metal hydride

Received: September 27, 2016
Published: December 20, 2016

DOI: 10.1021/jacs.6b10148
J. Am. Chem. Soc. 2017, 139, 239−244

complexes of first-row transition metals (Scheme 1B).[19,20] We have used this complex to probe the influence of acid pK_a, type and structure on the observed rate constant for PT (k_{PT}) in hydride formation. Our results demonstrate that the operating mechanism follows the ET-PT pathway. Surprisingly, the rate constant for the PT step shows a linear free energy relationship (LFER) with the pK_a of the proton source until *past* the point when the transfer becomes exergonic. The rate constant for PT becomes acid pK_a independent for stronger acids, at a value significantly below the diffusion limit. The effect of the acid structure is also highlighted by the tremendous impact of sterically bulky acids on k_{PT}.

RESULTS AND DISCUSSION

Characterization of [Co(Cp)(dppe)]$^{2+}$ in the Absence of a Proton Source. We employed electrochemistry to probe the reactivity of [Co(Cp)(dppe)(CH_3CN)]$(PF_6)_2$ in the presence of protons and electrons in acetonitrile (CH_3CN). Cyclic voltammograms (CVs) of a CH_3CN solution containing [Co(Cp)(dppe)(CH_3CN)]$(PF_6)_2$ show two reversible one-electron waves in the potential range studied (Figure 1, blue trace). The waves at −0.51 and −0.93 V vs Fc^+/Fc correspond to the Co(III/II) and Co(II/I) reductions with peak-to-peak separations of 62 and 61 mV at 100 mV/s, respectively. This qualitatively agrees with reports in dichloromethane for the Co(II/I) reductions,[20] and a related Cp* complex.[21] We sought to obtain a more quantitative description of the system to fully map out its behavior in CH_3CN. A diffusion coefficient of D = 3.4×10^{-6} cm^2/s was determined through a variable scan rate (υ) study using the Randles−Sevcik equation (see Supporting Information (SI)). This value is comparable with diffusion coefficients reported for other molecular cobalt complexes.[10,15,22] The heterogeneous electron transfer rate constant (k_s) was determined using working curves (see SI). The reduction of Co^{III} has a k_s of 0.051 cm/s, while the reduction of the Co^{II} has a k_s of 0.11 cm/s on the glassy carbon electrode used. Although cobalt (III/II) reduction couples generally are reported to undergo slow electron transfer,[15,23,24] the present value is an order of magnitude higher than for cobaloximes.[15] The faster electron transfer for the reduction of cobalt(II) echoes the behavior reported for cobalt hangman porphyrin systems[10] and is the same order of magnitude as ferrocene in CH_3CN.[25]

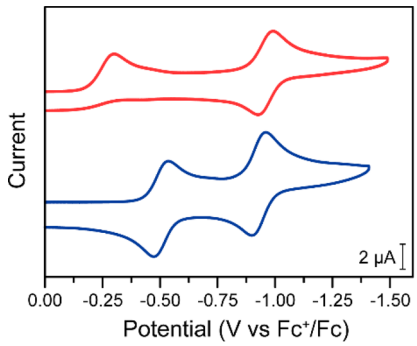

Figure 1. CVs of [Co(Cp)(dppe)(CH_3CN)]$(PF_6)_2$ in CH_3CN (0.5 mM, blue trace) and in CH_2Cl_2 (0.5 mM, red trace). The voltammograms were recorded at 100 mV/s in 0.25 M $[Bu_4N][PF_6]$.

CH_3CN Ligand Loss. In order to form the Co^{III} hydride species, the coordinated CH_3CN of the isolated Co^{III} species must dissociate. CVs recorded in CH_2Cl_2 provide insight into the ligand dissociation step (Figure 1, red trace). If decoordination of CH_3CN occurs in the Co^{III} oxidation state, the CH_3CN ligand would be irremediably lost upon dissolution of the complex in the CH_2Cl_2 electrolyte solution. In this scenario, the Co(III/II) wave would retain its reversibility in the CV. Should the CH_3CN ligand be lost in the Co^{II} oxidation state, an irreversible Co(III/II) wave should be observed in the CV. In the cathodic sweep, [Co(Cp)(dppe)(CH_3CN)]$^{2+}$ would be reduced to [CoCp(dppe)(CH_3CN)]$^+$, but only [CoCp(dppe)]$^+$ would be present for re-oxidation in the anodic sweep. For a ligand loss in the Co^{I} oxidation state, both waves would be irreversible. Experimentally, an irreversible Co(III/II) wave is observed in CH_2Cl_2, followed by a reversible Co(II/I) wave at −0.96 V vs Fc^+/Fc (Figure 1), suggesting an EC mechanism where ligand loss occurs in the Co^{II} oxidation state. Upon titration of CH_3CN to the CH_2Cl_2 solution, reversibility of the Co(III/II) is recovered, and the $E_{1/2}$ shifts toward the reversible Co(III/II) wave observed in CH_3CN (see SI). The shift of the reversible wave with addition of more CH_3CN confirms an EC mechanism, following Scheme 2. The rate constant for CH_3CN dissociation from the Co^{II} was determined ($k_d = 4 \times 10^7$ s^{-1}) by varying the scan rate in the absence of CH_3CN (see SI). This rate constant, coupled to the 420 mV difference in the $E_{1/2}$ of the two couples, indicates that the study of hydride formation will proceed following Scheme 1, unencumbered by ligand dissociation from [Co(Cp)(dppe)(CH_3CN)](PF_6).

Scheme 2

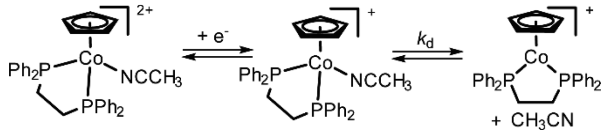

Evolution of CVs with Addition of Acid. When solutions of [Co(Cp)(dppe)(CH_3CN)]$(PF_6)_2$ in CH_3CN are treated with acid, the Co(II/I) reduction becomes irreversible, and the position of the peak shifts positive as the acid concentration is increased or when the acid pK_a is lowered (Figure 2). This behavior is typical of an EC reaction mechanism, where fast electron transfer (E) is followed by a rate-limiting chemical (C) step, and supports the assignment that hydride formation proceeds through the ET-PT pathway in these conditions (Scheme 3).

Diagnostic identification of an EC mechanism with CV includes the evolution of the peak potential with scan rate and the observed rate constant of the chemical step (k_{obs}), as well as the peak current and the peak width.[28] For hydride formation following a simple ET-PT pathway, the observed rate constant will take the form $k_{obs} = k_{PT}C_A$, where C_A is the concentration of acid and k_{PT} is the second-order rate constant for the PT step. For the reductive process studied, with external addition of substrate, the cathodic peak potential E_p shifts positively by 30 mV/dec with log([substrate]) and by −30 mV/dec with log(υ) according to[28]

$$E_p = E_{1/2} - \frac{RT}{F}(0.78) + \frac{RT}{2F}\ln\left(\frac{k_{obs}RT}{F\upsilon}\right)$$

where R, T, and F are the gas constant, temperature (in K), and Faraday's constant, respectively, and $E_{1/2}$ is the potential of the one-electron reversible electrochemical event in the absence of

DOI: 10.1021/jacs.6b10148
J. Am. Chem. Soc. 2017, 139, 239−244

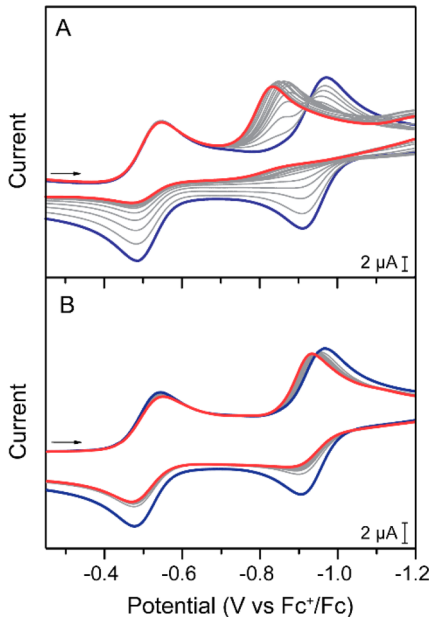

Figure 2. CVs of $[Co(Cp)(dppe)(CH_3CN)](PF_6)_2$ in the absence of a proton source (blue) and as (A) 4-cyano-anilinium (pK_a = 7)[26] or (B) benzoic acid (pK_a = 21.51)[27] is titrated into an CH_3CN solution (gray to red). The voltammograms were recorded at 100 mV/s in 0.25 M $[Bu_4N][PF_6]$.

Scheme 3

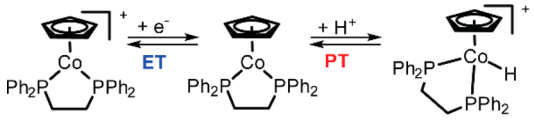

substrate. The evolution of the peak potential with C_A or υ affords straightforward determination of k_{PT}. A rate constant of k_{PT} = 1.8 × 10^7 M^{-1} s^{-1} is measured when using 4-cyano-anilinium as the acid (Figure 2A) and k_{PT} = 1.5 × 10^4 M^{-1} s^{-1} for benzoic acid (Figure 2B).

These measurements were repeated using acids spanning over 19 pK_a units (see SI). Figure 3 summarizes the k_{PT} values as a function of the acid source pK_a. The acids tested can be divided into three categories. For most acids of $pK_a \geq 16$, a linear free energy relationship is observed between $\log(k_{PT})$ and the pK_a of the proton source (Figure 3, red). For most acids with pK_a lower than ca. 14, k_{PT} is constant at ca. (2.1 ± 0.1) × 10^7 M^{-1} s^{-1} (Figure 3, green). The third group is composed of all remaining acids whose reactivity does not conform to the aforementioned trends (Figure 3, blue).

Influence of Acid Source on k_{PT}. For the acids of $pK_a \geq 16$, the rate constant increases as the acid pK_a is lowered. This general trend has been observed for the formation of bridging metal hydrides,[29,30] and recent reports have extended the LFER expected for a classical acid−base interaction between organic substrates to transition metal complexes.[13,23,31] In the present case, a LFER is observed between $\log(k_{PT})$ and pK_a with a slope of −0.55. This value is lower than LFERs measured in our group for the elementary proton transfer steps involved in hydrogen evolution catalyzed by a cobaloxime (−0.97 and −0.77 for the first and second steps, respectively) as measured through foot-of-the-wave and plateau current analysis under catalytic conditions. Of note, hydride formation was not rate-limiting under these conditions.[13,23] A LFER of −0.7 was observed for hydride protonation in a nickel-based catalyst.[31] Interestingly, the hydride protonation LFERs are quite similar for these two catalysts. However, the LFER associated with hydride formation for cobaloxime, determined under catalytic conditions, is closer to −1, nearly twice that of the model complex studied here. Understanding the significance of LFER slopes could provide crucial information to elementary reaction steps.

For acids in the two remaining groups, the evolution of k_{PT} with acid identity is less straightforward. The behavior of the acids of the third group (blue markers in Figure 3) is rationalized when examining the common structural features of these acids (**4**, **9**, **11**, and **14**). Notably, the acidic proton is sterically encumbered for all four acids. This suggests that the proton transfer kinetics between the acid and the Co^I center is impeded by steric interactions between the reactants, resulting in an attenuation of k_{PT}. Compared to the plateau region, the measured k_{PT} is up to 4 orders of magnitude lower in the case of 2,4,6-trimethylpyridinium (**9**).

For the strongest acids (pK_a < 14), the k_{PT} measured is acid pK_a independent, while k_{obs} still follows the general expression

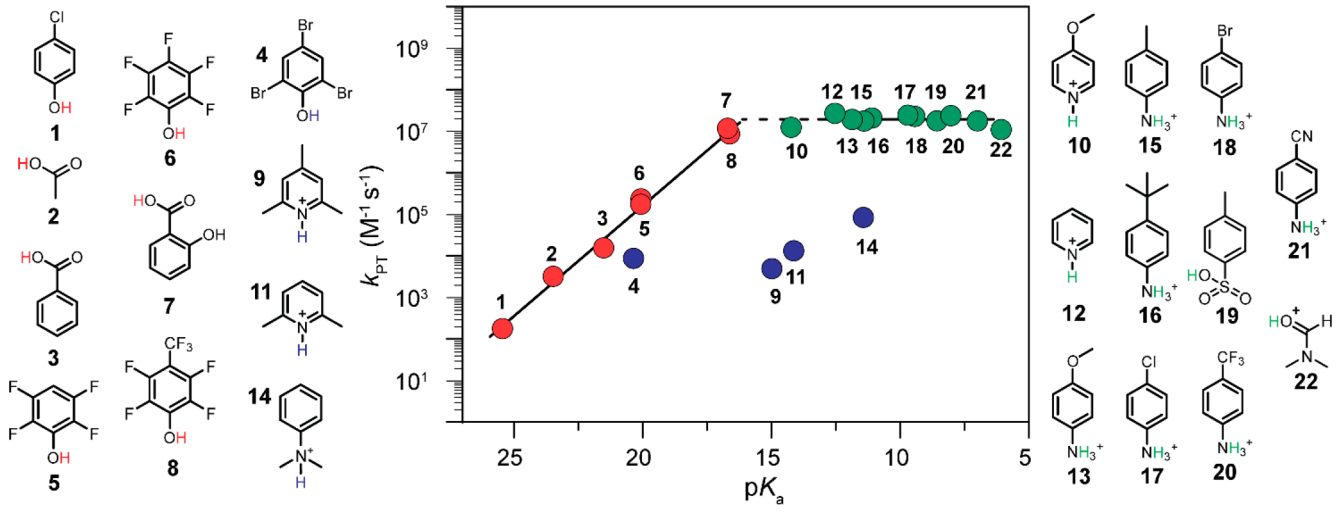

Figure 3. Rate constants for protonation of Co^I (k_{PT}) as a function of acid pK_a in CH_3CN.

DOI: 10.1021/jacs.6b10148
J. Am. Chem. Soc. 2017, 139, 239−244

$k_{obs} = k_{PT}C_A$. The value of k_{PT} in the plateau region, $(2.1 \pm 0.1) \times 10^7$ M^{-1} s^{-1}, is far below the diffusion limit, estimated at $k_{diff} = 1 \times 10^{10}$ M^{-1} s^{-1} using the Debye−Smoluchowski equation (see SI). This underscores the complexities of a step as seemingly simple as proton transfer. We have recognized that the driving force in the plateau region might be so strong that proton transfer is no longer rate-limiting in the formation of the cobalt hydride. In the context of hydride formation, the PT step free energy variation, ΔG°_{PT}, is related to the difference in pK_a between the proton source and the hydride.[32] The plot in Figure 3 thus relates the kinetic parameter k_{PT} to the thermodynamic value ΔG°_{PT}. The pK_a of this cobalt hydride was independently determined to be 18.4 through spectrophotometric titrations (see SI); as such, the LFER observed extends past the point where the reaction becomes exergonic, and $\Delta G^\circ_{PT} = -8.0$ kcal/mol for acid **12** and −15.6 kcal/mol for acid **21**. While identification of this new rate-limiting step is beyond the scope of this paper, we have considered a few explanations.

The observed reaction kinetics could result from a proton-independent pre-equilibrium before the protonation step or, alternatively, a proton-dependent equilibrium followed by an irreversible proton-independent step. In the former case, the k_{PT} measured is a product of the equilibrium constant and the rate constant for protonation. The plateau region would arise from the diffusion limit, with an estimate of the equilibrium constant at 10^{-3} (see SI). In the latter case, the plateau region could correspond to a shift in the kinetic control from the equilibrium protonation step to the acid-independent irreversible step while maintaining a dependence on proton concentration. Chemical identity of these steps could be a structural reorganization to accommodate for interaction with the acid source in the former case, and protonation of the Cp ring followed by intramolecular hydride formation in the latter case. Either scenario could yield an observed rate constant that is first order in acid, and further underscore the underlying complexity of hydride formation mechanisms.

Consequences for Catalyst Benchmarking. Together, these results highlight the importance of the choice of reaction conditions when evaluating hydrogen evolution catalysts. For example, if $[Co(Cp)(dppe)]^+$ was a catalyst for HER with rate-limiting hydride formation, choosing 4-cyano-anilinium or salicylic acid (acids **21** vs **7**) as a proton source would lead to a negligible increase in observed rate. However, the 10 pK_a-unit difference between the two conditions would correspond to a 572 mV increase in the overpotential for HER. The apparent reduction potentials in CH_3CN of the acids studied are tabulated in the SI to help guide future benchmarking studies. Similarly, reducing the proton source choice to pK_a considerations alone ignores the dramatic influence of sterics observed on the rate constant for hydride formation. The effect of steric bulk can be alleviated in systems containing a proton shuttle such as a water[33,34] or a proton relay built into the ligand,[35,36] although these approaches negate control of PT kinetics through acid pK_a. For other catalysts, the direct interaction of the acidic proton with the metal center in CH_3CN needs to be considered and highlights the role of sterics on the kinetics. This is exemplified by the 2 orders of magnitude difference of k_{PT} between 4-methylanilinium and *N*,*N*-dimethylanilinium (**14** and **15**) despite a 0.03 pK_a difference. Together, these results point to the benefit of minimizing steric effects when choosing an acid source for benchmarking purposes as well as understanding the relation between k_{PT} and pK_a and the possible presence of a plateau region. It is striking to note that the trends observed hold across all acid types tested: carboxylic acids, aniliniums, pyridiniums, phenols, and even acids with non-ideal behaviors in CH_3CN such as *p*-toluenesulfonic acid and dimethylformamidium. While steps were taken to keep heteroconjugation effects to a minimum with rigorous drying of all solvents and reagents, the influences of homoconjugation and dimerization appear to be limited in the conditions tested. The influence of dimerization of the acid source was tested with the use of salicylic acid (acid **7**), which has been reported to be prone to dimerizing.[37] The rate constant obtained is in line with that of 4-CF_3-2,3,5,6-F_4-phenol (acid **8**), emphasizing the negligible effect of this parameter in these conditions. Similarly, homoconjugation under these conditions is not a major factor, as exemplified by the results with salicylate, prone to homoconjugate, and pyridine and *p*-cyanoaniline, which are not.

CONCLUSIONS

In summary, using a model complex to decouple hydride formation from hydrogen evolution, we have demonstrated a complex relationship between rate constant for proton transfer and the pK_a of the proton source. A LFER for weaker acids confirmed the trade-off observed between rate of protonation and driving force for proton transfer. Transposing our results to catalytic HER systems highlights the delicate task of catalyst benchmarking. For catalysts limited by hydride formation rates,[6−11] the choice of acid could have a strong impact on the catalytic rates observed through the pK_a and structure of the proton source. For stronger acids, the increased pK_a could translate to higher overpotentials in a catalytic system without necessarily a corresponding rate increase. These results underscore the need to examine elementary reaction steps in detail, elucidate intrinsic catalytic activity, and investigate rate vs pK_a relationships.

EXPERIMENTAL METHODS

General Considerations. All experiments were performed in a nitrogen-filled glovebox unless otherwise noted. A Pure Process Technology solvent purification system was used to dry and degas solvents with argon: acetonitrile (Fisher Scientific, HPLC grade, >99.9%), diethyl ether (VWR, ACS reagents), toluene (VWR, ACS reagents), and dichloromethane (Fisher Scientific, GC/MS grade).

Nitromethane (Sigma-Aldrich, ACS reagent ≥95%) was degassed with three freeze−pump−thaw cycles before use. Tetrabutylammonium hexafluorophosphate (Acros Organics, 98%) was recrystallized as previously reported.[38] 1,2-Bis(diphenylphosphino)ethane (TCI America, >97%), dimethyl sulfide (Sigma-Aldrich, anhydrous ≥99%), and cyclopentadienylcobalt dicarbonyl (Strem, >95%) were used as received. Ferrocenium hexafluorophosphate was synthesized following a literature procedure.[39] Benzene-d_6 (99.5% D) and acetonitrile-d_6 (99.8% D) were purchased from Cambridge Isotope Laboratories. Triethylamine (Sigma-Aldrich, ≥99.5%) was freeze−pump−thawed and stored under N_2 over molecular sieves.

The complex $[CoCp(dppe)(CH_3CN)](PF_6)_2$ was synthesized following a literature procedure.[20]

Co(Cp)(dppe) was synthesized by modified literature procedures.[40] $Co(Cp)(CO)_2$ (250 μL, 1.87 mmol) and dppe (672 mg, 1.69 mmol) were dissolved in toluene (20 mL). The reaction vessel was then stirred at reflux under N_2 for 4 h. The solvent was removed in vacuo to afford a dark red residue. Acetonitrile (40 mL) was added to the residue, and the mixture was sonicated for 10 min. The fine red powder was then filtered, rinsed with CH_3CN (3 × 10 mL), and dried under high vacuum (468 mg, 53%). ^1H NMR (400 MHz, C_6D_6): δ

DOI: 10.1021/jacs.6b10148
J. Am. Chem. Soc. 2017, 139, 239−244

(ppm) 7.69 (m, 8H), 7.13−7.05 (m, 12H), 4.64 (s, 5H), 1.87−1.83 (m, 4H).

[HCo(Cp)(dppe)]BF_4 was synthesized according to the following procedure: 4-(methylbenzoate)-anilinium tetrafluoroborate[41] (45.5 mg, 0.190 mmol) was dissolved in CH_3CN (1 mL). This solution was added to Co(Cp)(dppe) (102 mg, 0.194 mmol), resulting in a clear, yellow-orange solution. This solution was split and added dropwise to three separate vials of diethyl ether (20 mL each), resulting in a sticky yellow solid. The vials were sonicated for 5 min, and the fine yellow solid was filtered, rinsed with diethyl ether (3 × 5 mL), and dried under high vacuum (97.6 mg, 84%). ^{1}H NMR (400 MHz, CD_3CN): δ (ppm) 7.73−7.45 (m, 20H), 5.03 (s, 5H), 2.62−2.31 (m, 4H), −15.32 (t, J_{PH} = 70.0 Hz, 1H).

Acids used in this study were prepared and purified according to previously published procedures. The tetrafluoroborate salts were used for the following acids: 4-cyanoanilinium,[41] 4-trifluoromethylanilinium,[23] 4-bromoanilinium,[41] 4-chloroanilinium,[41] 4-*tert*-butylanilinium,[41] 4-methylanilinium,[31] *N*,*N*-dimethylanilinium,[41] 4-methoxyanilinium,[41] pyridinium,[42] 2,6-dimethylpyridinium,[42] 4-methoxypyridinium,[42] 2,4,6-trimethylpyridinium,[42] and 4-(methylbenzoate)-anilinium.[23] The following neutral acids were purchased from commercial sources: 4-trifluoromethyl-2,3,5,6-tetrafluorophenol, 4-chlorophenol, pentabromophenol, pentafluorophenol, 2,4,6-tribromophenol, 2,3,5,6-tetrafluorophenol, glacial acetic acid, *p*-toluenesulfonic acid monohydrate, salicylic acid, and benzoic acid. The triflate salt of dimethylformamidium was used.[41]

Electrochemical Methods. Electrochemistry was performed in a nitrogen-filled glovebox with a WaveDriver potentiostat using glassy carbon working electrodes, a glassy carbon counter electrode, and a silver wire pseudo-reference electrode. A 20 mL scintillation vial was used as electrochemical cell, fitted with a custom-made Teflon cap to hold the three electrodes. The electrode leads in the glovebox were connected to the WaveDriver with a custom shielded electrode cable feedthrough. All scans were referenced to the ferrocenium/ferrocene couple at 0 V. Ferrocene was present in each scan unless otherwise noted. Ohmic drop was minimized using a high electrolyte concentration (0.25 M [Bu_4N][PF_6]), as well as by minimizing the distance between the working and reference electrodes. The residual ohmic drop was compensated using the method developed by Pine Research Instrumentation for the WaveDriver. Glassy carbon electrodes (CH Instruments, 3 mm diameter disk) were polished with 0.05 μm alumina powder (CH Instruments, contained no agglomerating agents) Milli-Q water slurries, rinsed, and ultrasonicated briefly in Milli-Q water to remove residual polishing powder. The pseudo-reference silver wire electrode was submerged in a glass tube containing electrolyte (0.25 M [Bu_4N][PF_6] in CH_3CN or CH_2Cl_2) and separated from the solution with a porous glass Vycor tip. The working electrode was pretreated with cyclical scans from approximately 0.5 to −3 V (the exact value varied in accordance with the silver wire pseudo-reference) at 250 mV/s in 0.25 M [Bu_4N][PF_6] until cycles were superimposable (usually three cycles).

Optical Measurements. UV/vis absorbance spectra were obtained in a nitrogen-filled glovebox using an OceanOptics DH-mini light source fiber coupled to an OceanOptics Flame spectrometer, in a 1 cm path length quartz cuvette.

■ ASSOCIATED CONTENT

Supporting Information

The Supporting Information is available free of charge on the ACS Publications website at DOI: 10.1021/jacs.6b10148.

Further experimental details, CVs used for the determination of k_{PT}, as well as analysis of the CVs obtained in the absence of acid in CH_3CN and CH_2Cl_2 (PDF)

■ AUTHOR INFORMATION

Corresponding Author

*dempseyj@email.unc.edu

ORCID

Noémie Elgrishi: 0000-0001-9776-5031

Jillian L. Dempsey: 0000-0002-9459-4166

Notes

The authors declare no competing financial interest.

■ ACKNOWLEDGMENTS

This work was supported by the U.S. Department of Energy, Office of Science, Office of Basic Energy Sciences, under Award No. DE-SC0015303, and the University of North Carolina at Chapel Hill. J.L.D. acknowledges support from a David & Lucile Packard Foundation Fellowship in Science and Engineering. We acknowledge Brian D. McCarthy for the synthesis of acids used in this study.

■ REFERENCES

(1) Huynh, M. H. V; Meyer, T. J. *Chem. Rev.* **2007**, *107*, 5004.
(2) Cook, T. R.; Dogutan, D. K.; Reece, S. Y.; Surendranath, Y.; Teets, T. S.; Nocera, D. G. *Chem. Rev.* **2010**, *110*, 6474.
(3) Solis, B. H.; Hammes-Schiffer, S. *Inorg. Chem.* **2014**, *53*, 6427.
(4) Weinberg, D. R.; Gagliardi, C. J.; Hull, J. F.; Murphy, C. F.; Kent, C. A.; Westlake, B. C.; Paul, A.; Ess, D. H.; McCafferty, D. G.; Meyer, T. J. *Chem. Rev.* **2012**, *112*, 4016.
(5) Bourrez, M.; Steinmetz, R.; Ott, S.; Gloaguen, F.; Hammarström, L. *Nat. Chem.* **2015**, *7*, 140.
(6) Artero, V.; Saveant, J.-M. *Energy Environ. Sci.* **2014**, *7*, 3808.
(7) Razavet, M.; Artero, V.; Fontecave, M. *Inorg. Chem.* **2005**, *44*, 4786.
(8) Helm, M. L.; Stewart, M. P.; Bullock, R. M.; DuBois, M. R.; DuBois, D. L. *Science* **2011**, *333*, 863.
(9) Dempsey, J. L.; Brunschwig, B. S.; Winkler, J. R.; Gray, H. B. *Acc. Chem. Res.* **2009**, *42*, 1995.
(10) Roubelakis, M. M.; Bediako, D. K.; Dogutan, D. K.; Nocera, D. G. *Energy Environ. Sci.* **2012**, *5*, 7737.
(11) Bediako, D. K.; Solis, B. H.; Dogutan, D. K.; Roubelakis, M. M.; Maher, A. G.; Lee, C. H.; Chambers, M. B.; Hammes-Schiffer, S.; Nocera, D. G. *Proc. Natl. Acad. Sci. U. S. A.* **2014**, *111*, 15001.
(12) Elgrishi, N.; Chambers, M. B.; Fontecave, M. *Chem. Sci.* **2015**, *6*, 2522.
(13) Elgrishi, N.; McCarthy, B. D.; Rountree, E. S.; Dempsey, J. L. *ACS Catal.* **2016**, *6*, 3644.
(14) Rountree, E. S.; Dempsey, J. L. *J. Am. Chem. Soc.* **2015**, *137*, 13371.
(15) Wiedner, E. S.; Bullock, R. M. *J. Am. Chem. Soc.* **2016**, *138*, 8309.
(16) Lee, C. H.; Dogutan, D. K.; Nocera, D. G. *J. Am. Chem. Soc.* **2011**, *133*, 8775.
(17) Huo, P.; Uyeda, C.; Goodpaster, J. D.; Peters, J. C.; Miller, T. F. *ACS Catal.* **2016**, *6*, 6114.
(18) McKone, J. R.; Marinescu, S. C.; Brunschwig, B. S.; Winkler, J. R.; Gray, H. B. *Chem. Sci.* **2014**, *5*, 865.
(19) Wiedner, E. S.; Chambers, M. B.; Pitman, C. L.; Bullock, R. M.; Miller, A. J. M.; Appel, A. M. *Chem. Rev.* **2016**, *116*, 8655.
(20) Koelle, U.; Paul, S. *Inorg. Chem.* **1986**, *25*, 2689.
(21) Nagasawa, T.; Nagata, T. *Biochim. Biophys. Acta, Bioenerg.* **2007**, *1767*, 666.
(22) Elgrishi, N.; Chambers, M. B.; Artero, V.; Fontecave, M. *Phys. Chem. Chem. Phys.* **2014**, *16*, 13635.
(23) Rountree, E. S.; Martin, D. J.; McCarthy, B. D.; Dempsey, J. L. *ACS Catal.* **2016**, *6*, 3326.
(24) Gaddie, R. S.; Moss, C. B.; Elliott, C. M. *Langmuir* **2013**, *29*, 825.
(25) Kadish, K. M.; Ding, J. Q.; Malinski, T. *Anal. Chem.* **1984**, *56*, 1741.
(26) Appel, A. M.; Lee, S.; Franz, J. A.; Dubois, D. L.; Dubois, M. R.; Twamley, B. *Organometallics* **2009**, *28*, 749.

DOI: 10.1021/jacs.6b10148
J. Am. Chem. Soc. 2017, 139, 239−244

(27) Kütt, A.; Leito, I.; Kaljurand, I.; Sooväli, L.; Vlasov, V. M.; Yagupolskii, L. M.; Koppel, I. A. *J. Org. Chem.* **2006**, *71*, 2829.
(28) Savéant, J.-M. *Elements of Molecular and Biomolecular Electrochemistry*; John Wiley & Sons, Inc.: Hoboken, NJ, 2006.
(29) Mirmohades, M.; Pullen, S.; Stein, M.; Maji, S.; Ott, S.; Hammarström, L.; Lomoth, R. *J. Am. Chem. Soc.* **2014**, *136*, 17366.
(30) Jablonskytė, A.; Webster, L. R.; Simmons, T. R.; Wright, J. A.; Pickett, C. J. *J. Am. Chem. Soc.* **2014**, *136*, 13038.
(31) Rountree, E. S.; Dempsey, J. L. *Inorg. Chem.* **2016**, *55*, 5079.
(32) Warren, J. J.; Tronic, T. A.; Mayer, J. M. *Chem. Rev.* **2010**, *110*, 6961.
(33) Jackson, M. N.; Surendranath, Y. *J. Am. Chem. Soc.* **2016**, *138*, 3228.
(34) Bonin, J.; Costentin, C.; Louault, C.; Robert, M.; Savéant, J. M. *J. Am. Chem. Soc.* **2011**, *133*, 6668.
(35) Loewen, N. D.; Thompson, E. J.; Kagan, M.; Banales, C. L.; Myers, T. W.; Fettinger, J. C.; Berben, L. A. *Chem. Sci.* **2016**, *7*, 2728.
(36) O'Hagan, M.; Shaw, W. J.; Raugei, S.; Chen, S.; Yang, J. Y.; Kilgore, U. J.; DuBois, D. L.; Bullock, R. M. *J. Am. Chem. Soc.* **2011**, *133*, 14301.
(37) Izutsu, K. *Acid-Base Dissociation Constants in Dipolar Aprotic Solvents*; IUPAC Chemical Data Series; Blackwell Science: Oxford, UK, 1990.
(38) McCarthy, B. D.; Donley, C. L.; Dempsey, J. L. *Chem. Sci.* **2015**, *6*, 2827.
(39) Breuer, R.; Schmittel, M. *Organometallics* **2012**, *31*, 1870.
(40) Koelle, U.; Paul, S. *Inorg. Chem.* **1986**, *25*, 2689.
(41) McCarthy, B. D.; Martin, D. J.; Rountree, E. S.; Ullman, A. C.; Dempsey, J. L. *Inorg. Chem.* **2014**, *53*, 8350.
(42) McCarthy, B. D.; Dempsey, J. L. *Inorg. Chem.* **2017**, DOI: 10.1021/acs.inorgchem.6b02325.

DOI: 10.1021/jacs.6b10148
J. Am. Chem. Soc. 2017, 139, 239–244